PCCP

ROYAL SOCIETY OF CHEMISTRY

PAPER

View Article Online
View Journal | View Issue

Cite this: *Phys. Chem. Chem. Phys.*, 2025, **27**, 14565

Left–right asymmetry in the microstructure of the hindwings of European hornet revealed by scanning electron microscopy and microscopic vibrational circular dichroism†

Sayako Inoué, *[ab] Hisako Sato [c] and Akihiko Yamagishi[d]

Received 15th March 2025,
Accepted 12th June 2025

DOI: 10.1039/d5cp01013f

rsc.li/pccp

Observation of hornet hindwings using scanning electron microscopy revealed a coating composed of helically wound hairs of approximately 10 μm in diameter and 100 μm in length. A strict enantiomeric relationship in the organ morphology existed in the area closest to the leading edge of the wings: the hairs on the right wing exhibited left-handedness, whereas those on the left wing exhibited right-handedness. Evaluation of microscopic vibration circular dichroism spectra indicated that both sides of the wings comprised β-sheets. However, a notable difference in VCD spectral shapes existed between the left and right wings (VCD_{left} and VCD_{right}, respectively), although their IR spectra were nearly identical. From the spectral shape of the difference ($VCD_{left} - VCD_{right}$), one possibility is proposed that the handedness in the hairs on the left and right hindwings is related to the opposite chirality of the protein structure. The correlation between organ-level enantiomeric relationships and the protein secondary structure observed here is a novel observation that requires further investigation to obtain deeper insights.

Introduction

Left–right asymmetry is ubiquitous in animals. Chirality is one of the main aspects of left–right asymmetry in animal organs. When an object or system is not superimposable on its mirror image, it is considered chiral. Common examples of chirality found in animals include the internal organs of humans, the coiling of snail shells,[1,2] and the visceral organs of *Drosophila*.[3–6] The chiral structures of biological systems are formed of chiral organic molecules that serve as building blocks, such as amino acids and sugars.[7] These building blocks are homochiral: the amino acids in proteins are almost exclusively left-handed L-amino acids, and most sugars in DNA and RNA are right-handed D-glucose.[8–10] One issue that has caught the attention of researchers is how chiral organs are formed by such homochiral building blocks. However, at present, this remains poorly understood. Organ-level chirality is common among insects. Enantiomeric pairs of left and right wings allow flapping flight, gliding, and hovering.[11,12] The primary component of the insect wing is the cuticle.[13] The cuticle is a multi-layered material composed of chitin embedded in proteins.[14,15] The relationship between visible chirality in insect organs and molecular properties, such as the secondary structure of component proteins, is crucial for understanding the origin of left–right asymmetry. In addition to the layout of insect wings, the microstructures on their surfaces, such as arrays of bumps, scales, and hairs, are responsible for their functionality.[16,17] It can be assumed that the microstructures on the left and right wings are also enantiomeric. However, this hypothesis has not been adequately investigated. Vibrational circular dichroism (VCD) is a technique that is capable of determining the absolute configuration of chiral molecules.[18,19] VCD was used to determine the supramolecular chirality of biomacromolecules.[20–23] Recently, we successfully determined the secondary structure of proteins in insect wings using a multidimensional vibrational circular dichroism (denoted as MultiD-VCD) system with a spatial resolution of 100 μm.[24–27] Using the MultiD-VCD technique, we revealed that the forewings of the European hornet *Vespa crabro flavofasciata* consisted of segregated domains of proteins with α-helical and β-sheet structures.[24] In this study, we characterised hair-like microstructures on the left and right hindwings of *Vespa crabro flavofasciata* using scanning electron microscopy (SEM) to determine the helical grooves on their surfaces. The secondary protein structure of insect wings containing the

[a] *Geodynamics Research Center (GRC), Ehime University, Matsuyama, 790-8577, Japan. E-mail: inoue.sayako.nr@ehime-u.ac.jp; Tel: +81-89-927-8611*
[b] *International Institute for Sustainability with Knotted Chiral Meta Matter (WPISKCM²), Hiroshima University, Higashi-Hiroshima, 739-8526, Japan*
[c] *Faculty of Science, Ehime University, Matsuyama, 790-8577, Japan*
[d] *Faculty of Medicine, Toho University, Tokyo, 143-8540, Japan*

† Electronic supplementary information (ESI) available: Number of left- and right-handed helical groove observed (Table S1); detailed characterization of morphology of microtrichia (Tables S2, S3 and Fig. S2–S7); supporting IR and VCD data (Fig. S1, S8 and S9). See DOI: https://doi.org/10.1039/d5cp01013f

microstructures was determined using MultiD-VCD. The handedness of the groove showed an enantiomeric relationship between the left and right hindwings. Similar handedness was observed in the vibrational properties of the hindwings, as measured by the VCD. Taken together, these findings suggest that the enantiomeric relationship observed in the microtrichia structure is related to the α-helices of proteins. These results provide a basis for understanding the origin of chirality in insect organs.

Experimental methods

Insect wing sampling

The left and right hindwings of *Vespa crabro flavofasciata* Cameron 1903 (female) were dissected from a dead specimen collected in Imabari, Japan, which was provided by the Biodiversity Center, Ehime Prefectural Institute of Public Health and Environmental Science. The specimen is an endangered species.

SEM

Both sides of the wing surfaces were coated with gold using a JEOL JFC-1600 coater at a sputtering current of 20 mA for 60 seconds. The samples were observed using a field-emission scanning electron microscope (JSM-IT500HR, JEOL, Japan) operated at 3 kV. The SEM resolution is less than 1.5 nm. The obtained SEM images were analysed using Fiji (ImageJ).[28] The direction of the helices was determined from the SEM images. The length, diameter and pitch of the helices were measured from the hair on which the long axis appeared perpendicular to the viewing direction.

Microscopic vibrational circular dichroism based on quantum cascade laser (QCL-VCD) measurements

VCD spectra were measured using a machine developed in-house with the cooperation of JASCO Corporation, Japan (named MultiD-MIRAI-2020 spectrometer). The machine was a concurrent system combined with QCL-VCD (quantum cascade laser) covering the wavenumber range of 1500–1740 cm^{-1} and FT-VCD covering 800–2000 cm^{-1}. The monitoring infrared (IR) light from a quantum cascade laser was focused using two BaF_2 plano-convex lenses. The spatial resolution was 100 μm. To avoid water vapor disturbance, a cell compartment was purged by flowing dry N_2 at a rate of approximately 6 L min^{-1}. An N_2 gas generator (M2NT-0.4II-6, KOFLOC (Kyoto, Japan)) was used. A laser light source covers the wavenumber region assigned to the amide group of amino acids or peptides. The sample stage can be switched between normal and automatic scanning measurements. In this study, we used the QCL-VCD method with a microscopic automatic scanning function. The original data for the mapping experiments were obtained when the sample was scanned by an automatic micro-sampling accessory with focusing lenses. Initially, scanning was performed at a fixed wavenumber of 1650 cm^{-1} with an interval of 0.2–0.1 mm over a *ca.* 10 mm × 4 mm area. The areas of spectra acquisition for the detailed analyses described in the following are shown in Fig. S1 (ESI†). Next, a narrower area was scanned in the range of 1500–1740 cm^{-1} at a 0.1 mm interval within the area indicated by the open square in Fig. S1 (ESI†). In these mapping measurements, the sample stage was moved one- or two-dimensionally by 0.1 mm steps. The spectra were recorded by scanning over the wavenumber range of 1500–1740 cm^{-1} at a step of 1.0 cm^{-1}. The VCD spectra obtained at the same position on the left and right wings were paired. The pair was determined based on the position and whether the IR spectra of the left and right wings were identical.

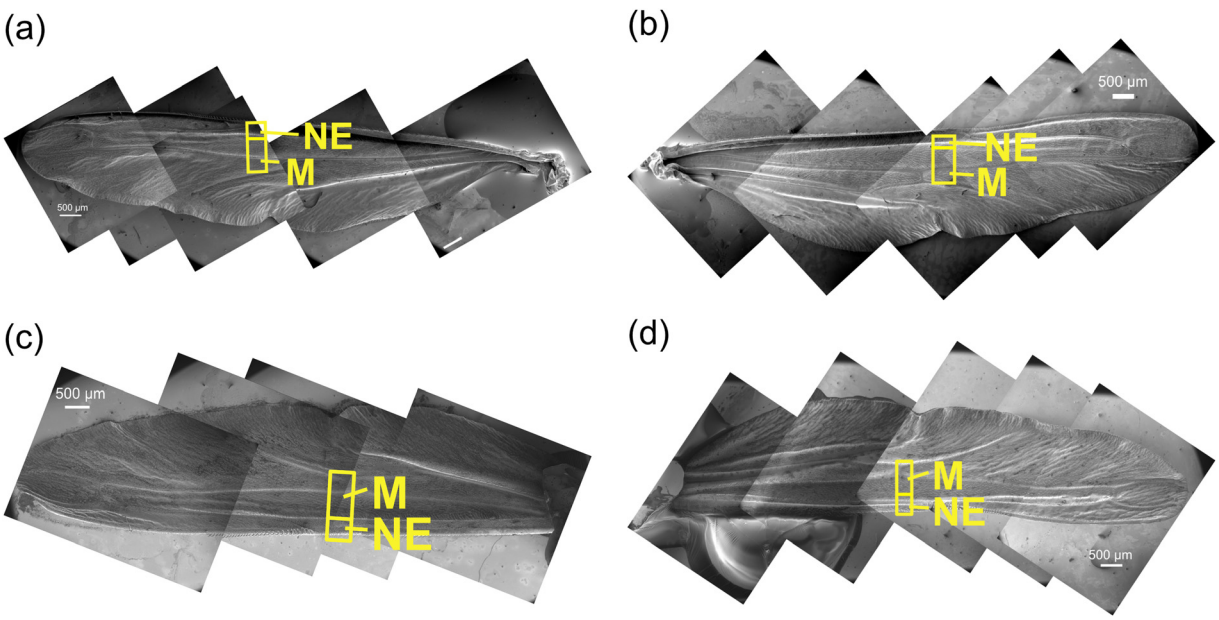

Fig. 1 (a) and (b) Mosaic of SEM images of the ventral surfaces of the (a) left and (b) right hindwings. (c) and (d) Mosaic of SEM images of the dorsal surfaces of the (c) left and (d) right hindwings. The open squares show the near-edge region (NE) and the medial region (M).

The IR and VCD signals were only accumulated once. The time required to perform measurements at each wavenumber was less than 4 s, and no baseline correction was performed. The data were treated by applying Savitzky–Golay smoothing with 13 points to reduce the noise level. Measurements were performed on the dorsal and ventral sides of the samples by rotating with respect to the monitoring laser light. No anisotropic artefact was observed. The QCL-VCD measurements were conducted on two pairs of left and right hindwings obtained from the two bodies of European hornets.

Results and discussion

The ventral and dorsal surfaces of the left and right hindwings were covered with an array of microscopic hair-like structures (*i.e.*, microtrichia) (Fig. 1). The diameter of the hair root was between 6 and 7 μm (average value of 6.6 μm). On the ventral surface, the microtrichia covered the membrane but were sparsely present on the surface of the vein. However, the distinction between the vein and membrane regions was unclear, and the microtrichia covered the entire dorsal surface of the wing. Microtrichia were found to grow in the apical direction of the hindwing. The venation and orientation of the microtrichia in the left and right hindwings were symmetric (Fig. 1). The position of the hair appeared similar on both sides of the wing. In the case of male *P. heteroptera* wings, the position of the hair was the same on both sides of the wing.[29]

A helical groove was observed on the surface of the microtrichia. The chordwise distributions of handedness on the ventral and dorsal surfaces of the left and right wings were investigated using SEM. One of the most striking characteristics observed was that the handedness of the hair in the area closest to the leading edge (marked as the near-edge region in Fig. 1) was aligned in one direction (Fig. 2, 3 and Table S1, ESI†). On the ventral surface, the groove in the near-edge region was right-handed on the left wing and left-handed on the right wing (Fig. 3). The number of helical turns in the helix ranged from 9 to 11 on the left wing and from 6 to 10 on the right wing. The average length of microtrichia was 87 μm in the left wing and 92 μm in the right wing (Table S2, ESI†). The hair length increased with increasing number of helical turns (Fig. S2, ESI†). The handedness of the spirals on the dorsal surface of the hindwings was similar to that observed on the ventral surface (Fig. 2, 3 and Table S1, ESI†). The right-handed spiral was dominant in the left hindwing, whereas the left-handed spiral was dominant in the right hindwing (Fig. 2 and 3). The number of helical turns in the helix ranged from 11 to 14 on the left wing and from 10 to 11 on the right wing. The average length of the microtrichia was 103 μm on the left wing and 88 μm on the right (Table S2, ESI†). Despite the large deviation in hair length (Fig. S1, ESI†), the length of the microtrichia in the near-edge region was considered the same on both the ventral and dorsal surfaces of the left and right hindwings.

In the medial region of the wing (marked as the medial region in Fig. 1), the handedness of the groove appeared to be the opposite of that in the near-edge region (Fig. 2 and Table S1, ESI†). However, the handedness was not as uniform as that in the near-edge region (Fig. 2 and Fig. S3, S4, ESI†). On the ventral surface of the left hindwing, the frequency of left-handed helices was slightly higher than that of right-handed helices (Fig. 2 and Table S1, ESI†). The length and number of turns of the hairs were almost the same regardless of the

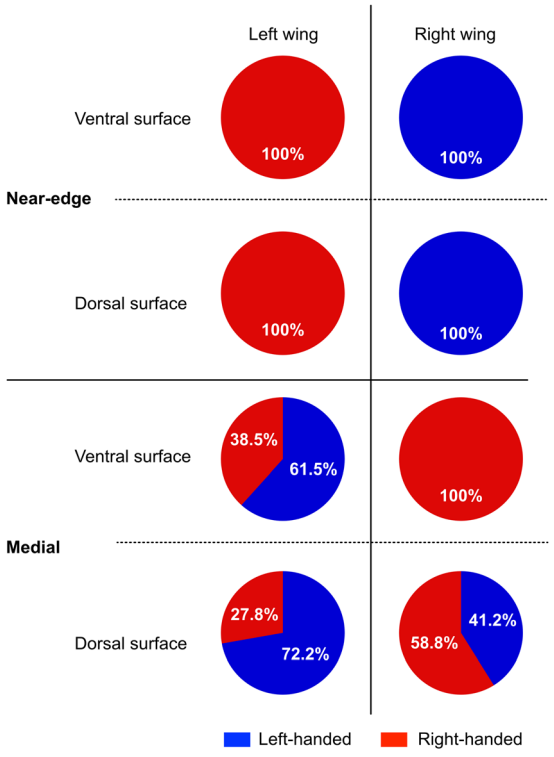

Fig. 2 Pie charts showing the frequency of left- and right-handed helical grooves observed in the near-edge and medial regions on the ventral and dorsal surfaces of the left and right hindwings. The number of microtrichia observed is shown in Table S1 (ESI†).

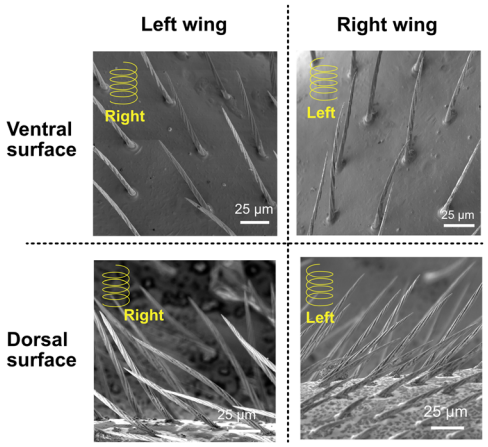

Fig. 3 SEM images of the helical groove on the microtrichia on the ventral and dorsal surfaces in the near-edge region of the left and right hindwings. The overlaid schematic indicates the handedness of the groove.

handedness of the helix. The average lengths were 91 μm for the left-handed hairs and 94 μm for the right-handed hairs (Table S2, ESI†). Only a right-handed helix was observed on the ventral surface of the right hindwing (Fig. 2 and Fig. S4, ESI†). The average length was 79 μm (Table S2, ESI†). Similar to the near-edge region, the trend in handedness on the dorsal surface was similar to that of the ventral surface (Fig. 2 and Fig. S5, S6, ESI†). Overall, the SEM observations suggest that the spatial distribution of handedness in the medial region is complex. The average hair length in the medial region of the dorsal surfaces was shorter than that in other parts of the hindwing. The average length of microtrichia on the left hindwing was 55 μm for left-handed helices and 59 μm for right-handed helices (Table S3, ESI†). That on the right hindwing was 44 μm for the left-handed helices and 51 μm for the right-handed helices (Table S3, ESI†). Regardless of the position and handedness of the hair, the pitch of the helix remained constant at approximately 2 μm (Fig. S7, ESI†). The diameters of the turns in the helix were not constant; the diameter was typically the longest between 1/3 and 1/2 the height from the root (Fig. S7, ESI†). The diameter trend indicated that the microtrichium had a slant-cone or arcuate shape. It is difficult to estimate the degree of curvature from SEM images because the viewing direction may not be perpendicular to the side of the hair. In summary, SEM observations revealed enantiomeric relationships in the microstructure of the left and right hindwing microtrichia. This relationship was clear in the near-edge region and less distinct in the medial region.

To identify protein structures, microscopic VCD measurements were performed in the same area as observed by SEM.

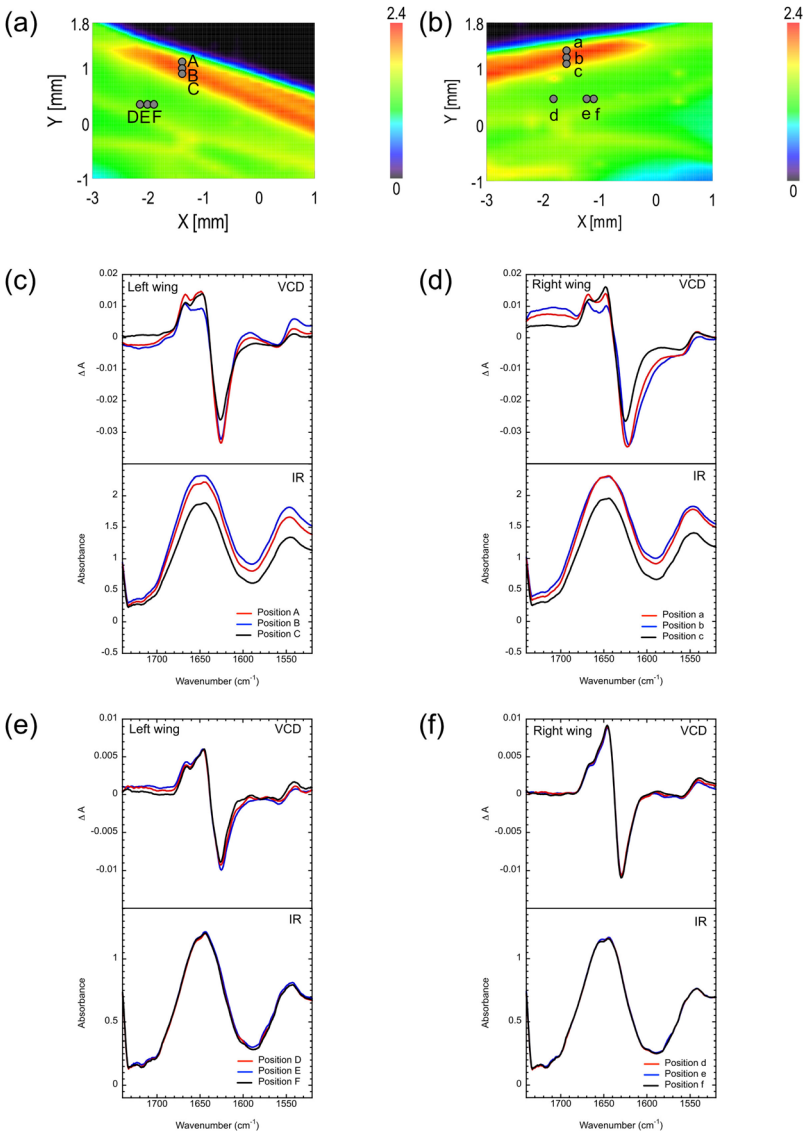

Fig. 4 (a) and (b) IR intensity maps at a fixed wavenumber of 1650 cm^{-1} of the left (a) and right (b) wings. The analyzed positions are indicated by the filled circles. Positions A–C and a–c are in the near-edge region. Positions D–F and d–f are in the medial region. (c) and (e) VCD and IR spectra obtained from the left wing. (d) and (f) VCD and IR spectra obtained from the right wing.

Fig. 4a and b show the IR maps of the left and right wings, respectively. The VCD and IR spectra obtained at the same positions on the left and right wings were compared. The positions A, B, and C in the near-edge region of the left-wing are paired with the positions a, b, and c of the right wing, respectively. Similarly, the positions D, E, and F in the near-edge region of the left-wing are paired with the positions d, e, and f in the right wing, respectively. The microscopic VCD has a spatial resolution of 100 μm. Based on the diameter of the microtrichium obtained from the SEM observations (6.6 μm on average), the VCD signals were the sum of at least two microtrichia and the membrane part. The VCD spectra showed distinctive positive bands around 1650 cm^{-1} and 1630 cm^{-1} (Fig. 4c and d). These spectral features are characteristic of the β-sheet structure of protein,[29,30] suggesting that the β-sheet was dominant in the analysed region. As the analysed area was mainly composed of a membrane, it is concluded that the membrane comprised the β-sheet. However, in the VCD spectra obtained in the near-edge region, the differences between the left and right wings in the VCD spectra were observed in the region between 1650 cm^{-1} and 1740 cm^{-1} (Fig. 4c and d). The IR spectra of the left and right wings were identical. To emphasize the difference in the VCD spectra, the difference curve between the left and right wings was obtained by subtracting the VCD spectra obtained on the right wing (VCD_{right}) from those obtained on the left wing (VCD_{left}) (Fig. S8, ESI†). The difference curves ($VCD_{left} - VCD_{right}$) of the near-edge region show a spectral feature that is different from that of the β-sheet. The SEM observations suggest that the left and right wings differ only in the microtrichia. This finding indicated that the spectral features of the differences curves were due to the differences in the microtrichia between the left and right wings. When the difference curve was compared with the VCD_{left} and VCD_{right} curves, the difference curve and VCD_{right} showed positive bands at 1720 cm^{-1} and 1660 cm^{-1}, whereas the VCD_{left} curve showed negative bands in the same region (Fig. 5a and Fig. S9a, b, ESI†). The spectral feature of the difference curve can be assigned to the right-handed α-helix[30,31] or the right-twisted β-sheet structure.[32] These spectral features are possible to be interpreted in terms of several mechanisms: (i) the amount of β-sheet in a membrane differed between the left- and right wings; (ii) the orientation of β-sheet axis in a membrane differed between these two wings; (iii) the handedness of the α-helix structure, which is assumed to exist in microtrichia, was opposite between these two wings. The definitive identification of handedness may be difficult because the strong spectral features of both α-helix and β-sheet were seen in the spectral region from 1600 to 1650 cm^{-1} (Fig. 5a). At the stage where no protein analysis has been performed in the microtrichia, it is difficult to determine which of the possibilities is probable.

In contrast to the near-edge region, the difference in the VCD_{left} and VCD_{right} was not visible in the medial region (Fig. 4e and f). The IR spectra of the left and right hindwings were identical. The difference spectrum shows the spectral features of the α-helix structure (Fig. 5b and Fig. S9c, d,

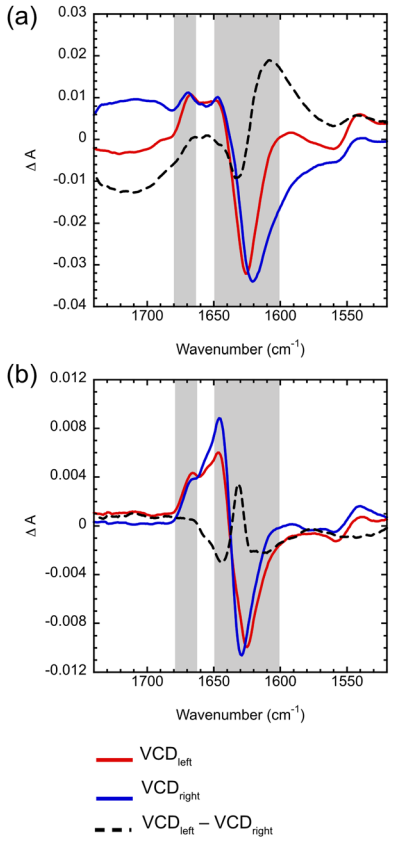

Fig. 5 (a) VCD spectra obtained from position A (VCD_{left}) and position a (VCD_{right}) wings and the difference of VCD_{left} and VCD_{right} ($VCD_{left} - VCD_{right}$). (b) VCD spectra obtained from position D (VCD_{left}) and position d (VCD_{right}) wings and the difference of VCD_{left} and VCD_{right} ($VCD_{left} - VCD_{right}$). The shaded region is the spectral region where the spectral feature of the β-sheet is pronounced.

ESI†).[29,30] As stated above, SEM observations revealed an enantiomeric relationship of the helical groove between the left and right wings in the near-edge region. However, in the medial region, the enantiomeric relationship is not as clear as that in the near-edge region. Taking the assumption that the morphological enantiomer pair is related to the α-helix structure, the trend observed by SEM explains why the differences in the VCD_{left} and VCD_{right} were only visible in the near-edge region. At the secondary structure level of naturally occurring proteins, right-handed helices are preferred to left-handed helices.[9,33] Although rare, left-handed helices can also occur.[33] Another possibility is the presence of differences in the multilevel hierarchical structures of proteins, such as coiled coils. The left-handed coiled coils, such as collagen and keratin, are built from the right-handed α-helix.[34,35] We anticipate that a more detailed characterization of the protein structure will provide more detailed information on the origin of morphological handedness.

Our study proposed that a combination of high-resolution SEM observations and microscopic VCD measurements is a powerful tool for characterizing left–right asymmetry in animals and investigating their origins. The presence of a microscale

enantiomeric relationship in insect wings may be more common than previously realized. As the microscopic characterization of organ-level chirality becomes more common, more species with microscale chirality will be described.

Conclusions

In summary, this study revealed an enantiomeric relationship between the smallest morphological features of the left and right hind wings. Herein, helically wound microtrichia were observed on the hindwings of European hornets using SEM. The handedness was found to be well-aligned near the leading edge of the wing; most of the microtrichia on the left wing had right-handed helical features, whereas those on the right wing had left-handed helical features. In the medial region, the handedness appeared to be less aligned. However, left- and right-handedness tended to be observed more frequently in the left and right wings, respectively. A comparison of the VCD spectra obtained from the left and right hindwings revealed that the handedness in the helically wound microtrichia was related to the chirality of the secondary protein structure. These findings demonstrate the feasibility of bottom-up construction of insect enantiomeric organ morphologies.

Author contributions

Sayako Inoué: conceptualisation, data curation, investigation (SEM), and writing – original draft; Hisako Sato: conceptualisation, data curation, investigation (IR, VCD), resources, funding acquisition, and writing – original draft; Akihiko Yamagishi: conceptualisation, investigation (IR, VCD), and writing – original draft.

Conflicts of interest

There is no conflict to declare.

Data availability

The data supporting this article have been included as part of the ESI.†

Acknowledgements

The authors are grateful to Mr Katsushi Narimatsu and Mr Yusuke Hara (Biodiversity Center, Ehime Prefectural Institute of Public Health and Environmental Science) for donating *Vespa crabro flavofasciata*. We are also indebted to Dr Toshiyuki Sasaki (Japan Synchrotron Radiation Research Institute) and Dr Yu Nishihara (Ehime University GRC) for supporting the analyses and Dr Taku Tsuchiya (Ehime University GRC) for valuable discussions. This study was supported by the Japan Society for the Promotion of Science (JSPS, KAKENHI (grant number JP22H02033)) and the Joint Usage/Research Center of the Premier Research Institute for UltraHigh-Pressure Sciences (PRIUS, Project No. 2023-D08) at Ehime University, Japan.

Notes and references

1 C. Grande and N. H. Patel, *Nature*, 2009, **457**, 1007–1011.
2 S. Urdy and R. Chirat, *J. Zool. Syst. Evol. Res.*, 2006, **44**, 1–7.
3 R. Kuroda, *Annu. Rev. Cell Dev. Biol.*, 2024, **40**, 97–117.
4 H. Taniguchi, M. He, P. Wu, S. Kim, R. Paik, K. Sugino, D. Kvitsani, Y. Fu, J. Lu and Y. Lin, *et al.*, *Neuron*, 2011, **71**, 995–1013.
5 P. Spéder, G. Ádám and S. Noselli, *Nature*, 2006, **440**, 803–807.
6 S. Hozumi, R. Maeda, K. Taniguchi, M. Kanai, S. Shirakabe, T. Sasamura, P. Spéder, S. Noselli, T. Aigaki and R. Murakami, *et al.*, *Nature*, 2006, **440**, 798–802.
7 P. Satir, *Philos. Trans. R. Soc., B*, 2016, **371**, 20150408.
8 J. Skolnick, H. Zhou and M. Gao, *Proc. Natl. Acad. Sci. U. S. A.*, 2019, **116**, 26571–26579.
9 S. Liu, *J. Phys. Chem. Lett.*, 2020, **11**, 8690–8696.
10 D. G. Blackmond, *Chem. Rev.*, 2019, **120**, 4831–4847.
11 S. Tahmasian and B. C. Kotulak-Smith, *Sci. Rep.*, 2024, **14**, 2814.
12 X. Cheng and M. Sun, *Sci. Rep.*, 2016, **6**, 25706.
13 E. Appel, J. Michels and S. N. Gorb, *Adv. Funct. Mater.*, 2024, **34**, 187–199.
14 J. F. Vincent and U. G. Wegst, *Anthropod. Struct. Dev.*, 2004, **33**, 187–199.
15 E. Atkins, *J. Biosci.*, 1985, **8**, 375–387.
16 G. S. Watson, B. W. Cribb and J. A. Watson, *ACS Nano*, 2010, **4**, 129–136.
17 G. Wen, Z. Guo and W. Liu, *Nanoscale*, 2017, **9** 3338–3366.
18 D. R. Hermann, G. Ramer, M. Kitzler-Zeiler and B. Lendl, *Anal. Chem.*, 2022, **94**, 10384–10390.
19 S. Lüdeke, M. Pfeifer and P. Fischer, *J. Am. Chem. Soc.*, 2011, **133**, 5704–5707.
20 M. Li, S. Jiang, X. Wang, W. Xu, C. Du, Y. Wei, X. Deng and M. Liu, *Angew. Chem., Int. Ed.*, 2024, **63**, e202411733.
21 D. Kurouski, J. D. Handen, R. K. Dukor, L. A. Nafie and I. K. Lednev, *Chem. Commun.*, 2014, **51**, 89–92.
22 D. Kurouski, R. A. Lombardi, R. K. Dukor, I. K. Lednev and L. A. Nafie, *Chem. Commun.*, 2010, **46**, 7154–7156.
23 A. Rodger, R. Marrington, D. Roper and S. Windsor, *ProteinLigand Interactions: Methods and Applications*, Humana Press, Totowa, NJ, 2005, pp. 343–363.
24 H. Sato, S. Inoué, J. Yoshida, I. Kawamura, J. Koshoubu and A. Yamagishi, *Phys. Chem. Chem. Phys.*, 2024, **26**, 17918–17922.
25 H. Sato, J. Koshoubu, S. Inoué, I. Kawamura and A. Yamagishi, *Chirality*, 2024, **36**, e23655.
26 H. Sato, A. Yamagishi, M. Shimizu, K. Watanabe, J. Koshoubu, J. Yoshida and I. Kawamura, *J. Phys. Chem. Lett.*, 2021, **12**, 7733–7737.
27 H. Sato, M. Shimizu, K. Watanabe, J. Yoshida, I. Kawamura and J. Koshoubu, *Anal. Chem.*, 2021, **93**, 2742–2748.
28 J. Schindelin, I. Arganda-Carreras, E. Frise, V. Kaynig, M. Longair, T. Pietzsch, S. Preibisch, C. Rueden, S. Saalfeld, B. Schmid, J.-Y. Tinevez, D. J. White, V. Hartenstein,

K. Eliceiri, P. Tomancak and A. Cardona, *Nat. Methods*, 2012, **9**, 676–682.
29 D. T. Polet, M. R. Flynn and F. A. Sperling, *PLoS One*, 2015, **10**, e0138282.
30 T. A. Keiderling, *Curr. Opin. Chem. Biol.*, 2002, **6**, 682–688.
31 A. Kurochka, J. Prša, J. Kessler, J. Kapitán and P. Bour, *Phys. Chem. Chem. Phys.*, 2021, **23**, 16635–16645.
32 D. Kurouski, R. K. Dukor, X. Lu, L. A. Nafie and I. K. Lednev, Spontaneous inter-conversion of insulin fibril chirality, *Chem. Commun.*, 2012, **48**, 2837–2839.
33 M. Novotny and G. J. Kleywegt, *J. Mol. Biol.*, 2005, **347**, 231–241.
34 A. Lupas, *Trends Biochem. Sci.*, 1996, **21**, 375–382.
35 B. Apostolovic, M. Danial and H.-A. Klok, *Chem. Soc. Rev.*, 2010, **39**, 3541–3575.